

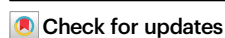


# Spatial correlation at the boson peak frequency in amorphous materials

Received: 26 June 2025

Accepted: 2 December 2025

Published online: 17 December 2025



X. Y. Li<sup>1,2,10</sup>, H. P. Zhang<sup>3,4,10</sup>, S. Lan<sup>5,6</sup>, D. L. Abernathy<sup>7</sup>, C. H. Hu<sup>1</sup>,  
L. R. Fan<sup>1</sup>, M. Z. Li<sup>3</sup> ✉ & X.-L. Wang<sup>1,6,8,9</sup> ✉

The Boson peak (BP), an excess of vibrational density of states, is ubiquitous for amorphous materials and is believed to hold the key to understanding the dynamics of glass and glass transition. Previous studies have established an energy scale for the BP, which is ~ 1-10 meV or ~ THz in frequency. However, so far, little is known about the momentum dependence or spatial correlation of the BP. Here, we report the observation of the BP in model Zr-Cu-Al metallic glasses over a wide range of momentum transfer, using inelastic neutron scattering, heat capacity, Raman scattering measurements, and molecular dynamics (MD) simulations. The BP energy is largely dispersionless; however, the BP intensity is found to scale with the static structure factor. Additional MD simulations with a generic Lennard-Jones potential confirm the same. Based on these results, an analytical expression for the dynamic structure factor is formulated for the BP excitation. Further analysis of the simulated disordered structures suggests that the BP is related to local structure fluctuations (e.g., in shear strain). Our results offer insights into the nature of the BP and provide guidance for the development of theories of amorphous materials.

Upon rapid cooling, liquids will solidify into non-equilibrium glassy or amorphous states<sup>1-3</sup>. As such, dynamic relaxation is a universal and intrinsic feature of glass and enables fluctuation and dissipation to occur<sup>4,5</sup>. Dynamic relaxation covers a broad range of time, length, and temperature scales, which in turn determines the properties and applications of glassy systems. As a result, there has been growing interest in the physics of glass<sup>6-13</sup>. Theoretically, the dynamical modes of glass can be clarified into two categories<sup>4</sup>. The first category pertains to transitions between adjacent basins or configurations within the potential energy landscape<sup>14</sup> encompassing the so-called  $\alpha$  and  $\beta$  relaxation processes. The second category involves the vibrational modes within a singular basin. The investigation of

vibrational modes holds significant importance due to its connection with the heat capacity and transport properties, such as thermal conductivity, which plays a crucial role in determining the performance of thermoelectric materials, as well as serving as a criterion for determining structural phase transitions in condensed matter<sup>15</sup>. In ordered crystals with long-range order, the vibrational modes manifest as plane-wave phonons, resulting in a vibrational density of states (VDOS)  $g(\omega)$  that adheres to Debye-like behavior at low frequencies<sup>16</sup>. In contrast, the VDOS of amorphous materials generally departs from the Debye form, exhibiting an excess of states known as the BP<sup>17,18</sup>. Following decades of intensive investigation, a consensus has formed that the BP is linked to specific sorts of

<sup>1</sup>Department of Physics, City University of Hong Kong; 83 Tat Chee Avenue, Hong Kong, China. <sup>2</sup>Beijing National Laboratory for Condensed Matter Physics, Institute of Physics, Chinese Academy of Sciences, Beijing, China. <sup>3</sup>School of Physics and Key Laboratory of Quantum State Construction and Manipulation (Ministry of Education), Renmin University of China, Beijing, China. <sup>4</sup>Songshan Lake Materials Laboratory, Dongguan, China. <sup>5</sup>Herbert Gleiter Institute of Nanoscience, School of Materials Science and Engineering, Nanjing University of Science and Technology; 200 Xiaolingwei Avenue, Nanjing, China. <sup>6</sup>Center for Neutron Scattering, City University of Hong Kong; 83 Tat Chee Avenue, Hong Kong, China. <sup>7</sup>Neutron Scattering Division, Oak Ridge National Laboratory, Oak Ridge, Tennessee, USA. <sup>8</sup>Hong Kong Institute for Advanced Sciences, City University of Hong Kong; 83 Tat Chee Avenue, Hong Kong, China. <sup>9</sup>City University of Hong Kong Shenzhen Research Institute; 8 Yuexing 1st Road, Shenzhen Hi-Tech Industrial Park, Shenzhen, China. <sup>10</sup>These authors contributed equally: X. Y. Li, H. P. Zhang. ✉ e-mail: [maozhili@ruc.edu.cn](mailto:maozhili@ruc.edu.cn); [xlwang@cityu.edu.hk](mailto:xlwang@cityu.edu.hk)

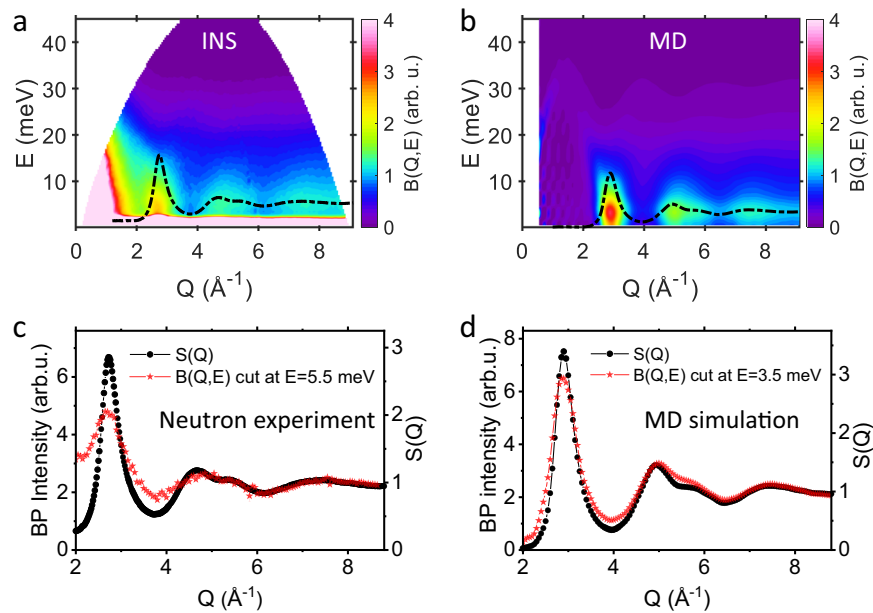


**Fig. 1 | Momentum dependence of the Boson peak (BP) in  $Zr_{46}Cu_{46}Al_8$  metallic glass (MG).** **a** Generalized  $Q$ -dependent density of states normalized by  $E^2$ ,  $B(Q, E)$ , measured by inelastic neutron scattering (INS) (see text). The strong INS intensity close to  $E = 0$  was due to the finite instrument resolution and the elastic scattering. **b** Molecular dynamics (MD) simulation results for  $B(Q, E)$ . The INS data show a well-defined BP around 5.5 meV, which is largely dispersionless as a function of  $Q$ . The static structure factor  $S(Q)$  is superimposed (the black dashed lines in **a** and **b**).

**c, d** The constant  $E$  cut plots at the BP energy (over  $\Delta E = 0.5$  meV) were superimposed with the experimental  $S(Q)$ . The INS intensity at the BP energy exhibits an excellent correlation with  $S(Q)$ . The error bars in **(c)** are estimated from the uncertainties of the measurement produced by the instrument software and propagated using the appropriate equation. Source data are provided in the Source Data file.

disorder<sup>13,19–22</sup>; however, the underlying structural mechanism of the BP has remained enigmatic and a subject of intense debate because the lack of translational periodicity precludes the use of well-established concepts in crystals.

Experimentally, the BP can be identified not only in the form of a broad peak in the specific heat data<sup>18,23</sup> but also in the VDOS, which can be measured by Raman scattering<sup>18,24,25</sup>, inelastic neutron scattering (INS)<sup>19,26</sup>, and inelastic x-ray scattering (IXS)<sup>27,28</sup>. Indeed, the early evidence for the BP was reported in the Raman spectra of vitreous  $SiO_2$  ( $\nu$ - $SiO_2$ ) by Krishnan<sup>29</sup>, who noted an extra broad-band (10–120  $cm^{-1}$ , or 1–15 meV) in comparison with its crystalline counterpart. It was (later) termed BP because the temperature dependence of the Raman intensity was thought to follow that of a harmonic oscillator characterized by the Bose factor<sup>17,18</sup>. The BP and BP-related phenomena were brought under the spotlight when Zeller and Pohl<sup>30</sup> pointed out the similarity in the anomalous behaviors of thermal conductivity and specific heat for several different families of glass<sup>17,18</sup>. Today, BP has been widely observed in various amorphous materials, ranging from metallic glasses (MGs)<sup>31,32</sup>, polymer and molecular glasses<sup>19,24,27,33,34</sup>, oxide and chalcogenide glasses<sup>17,21,35–38</sup>, ionic salt and bio-matter glasses<sup>39,40</sup>, colloidal and granular glasses<sup>22,41</sup>, model glasses<sup>13,20,42–44</sup>, confined water<sup>45,46</sup>, molecular crystal and strain glass<sup>47,48</sup>, van der Waals liquids<sup>49</sup>, and spin glass<sup>50</sup>, in spite of the very different interactions and structures in these materials.

Considerable studies have been carried out to explore the physical origin of the BP<sup>13,20,22,36,42,43,51–54</sup>. In general, there are two schools of thought regarding the origin of the BP. In the first view, the BP is considered a fingerprint of glass, i.e., an excess mode arising from the disordered atomic packing in amorphous materials<sup>13,42,52</sup>. In the second view, the DOS of the amorphous system is regarded as a modification of the crystalline DOS due to a random fluctuation of the force constants<sup>22,36,53</sup>. The controversy surrounding BP has lasted for decades, constituting one of the most fascinating and difficult puzzles in condensed matter physics and materials science.

In our view, this controversy is mainly caused by the incomplete definition of BP. In condensed matter, an elementary excitation is generally defined with two parameters, i.e., energy and momentum – their dynamic response functions describe the temporal and spatial correlation, respectively<sup>16</sup>. For the BP, past efforts have focused on the energy scale, while few studies were devoted to understanding the momentum dependence or spatial correlation at the BP energy. In 1984, Buchenau et al. studied the dynamic structure factor  $S(Q, E)$  around the BP energy in  $\nu$ - $SiO_2$  using INS and attributed the BP to the localized rotation motion of  $SiO_4$  tetrahedra<sup>55–57</sup>. About 15 years later, Nakamura and Arai et al. extended  $S(Q, E)$  measurements in  $\nu$ - $SiO_2$  to a larger  $Q$  range using then state-of-the-art time-of-flight spectrometer MARI at the ISIS spallation neutron source facility<sup>58,59</sup> and reported a non-dispersive behavior of the BP<sup>58</sup>. Recently, using MD simulations, Tanaka et al. also found the non-dispersive nature of the BP in a 2D model glass in a small range of  $Q$ , within the first sharp diffraction peak of the static structure factor  $S(Q)$ , and attributed it to localized transverse motion of chains<sup>13,42</sup>. The BP and phonon modes in glasses at small  $Q$  were also investigated by IXS<sup>17,38,60</sup>. There are, however, some discrepancies between the INS measured non-dispersive BP and the IXS data, which were attributed to the overlap between acoustic phonon modes and BP at small  $Q$ <sup>17,60</sup>. Therefore, the characterization and elucidation of the momentum dependence of the BP in amorphous materials is far from complete, impeding fundamental understanding of the physical origin of the BP. Here, we report a concerted investigation combining the powerful INS and MD simulations. We systematically characterize the momentum dependence of the BP over a large range of  $Q$  values in  $Zr_{46}Cu_{46}Al_8$  and  $Zr_{56}Cu_{36}Al_8$ , two typical MGs with very different glass-forming abilities. The dispersionless feature of the BP energy, independent of the momentum transfer  $Q$ , is observed in both INS and MD simulations. Moreover, the momentum dependence of the BP intensity is found to quantitatively scale with the  $S(Q)$  – this is not observed for excitations at other energies. MD simulations further suggest that the fluctuation of the local atomic shear

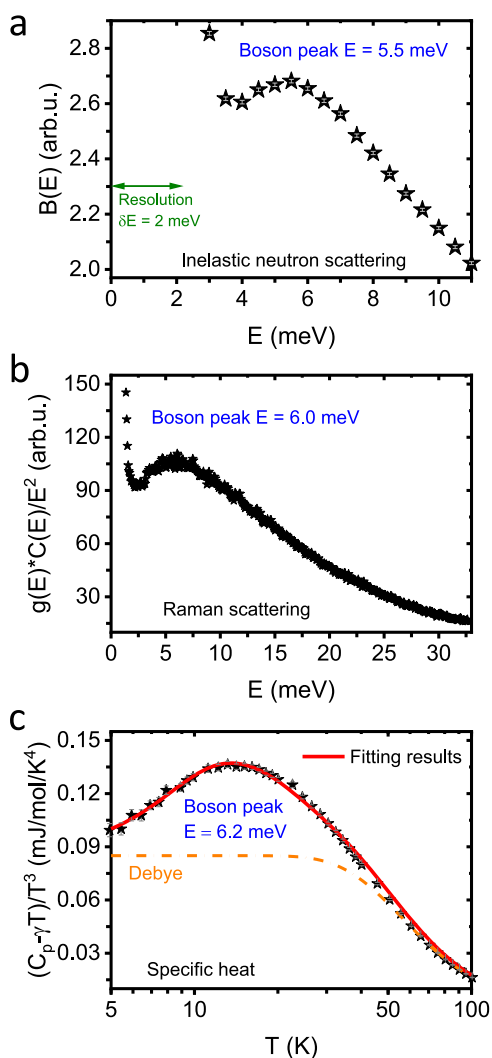


**Fig. 2 | BP in  $Zr_{46}Cu_{46}Al_8$  MG.** **a** The INS measured vibrational density of states normalized by  $E^2$ ,  $B(E)$ , showing a BP at  $\sim 5.5$  meV. Within the Debye model,  $B(E)$  would appear as a straight line at small  $E$  values. **b** The vibrational density of states normalized by  $E^2$ ,  $g(E) \cdot C(E)/E^2$ , where  $C(E)$  is a constant, obtained from the Raman scattering data, showing a BP around 6.0 meV. **c** The specific heat data presented as  $(C_p - \gamma T)/T^3$  vs  $T$ , which was fitted by the Einstein oscillator model (see “Methods”). The Debye level (the orange dash dot line) is plotted for reference. The fitted energy value using the Einstein oscillator mode was  $\sim 6.2$  meV. The error bars are estimated from the uncertainties of the measurement produced by the respective instrument software and propagated using the appropriate equation, and most of them are smaller than the size of the symbols. Source data are provided in the Source Data file.

strain is responsible for the BP, because it exclusively reproduces both distinct BP features mentioned above.

## Results

The INS measurements were performed at room temperature (RT) using ARCS<sup>61</sup> at the Spallation Neutron Source (SNS) to measure the VDOS in  $Zr_{46}Cu_{46}Al_8$  and  $Zr_{56}Cu_{36}Al_8$  MGs<sup>62,63</sup>. The high flux brought forth by the source power, coupled with advances in neutron instrumentation, has enabled high-precision measurements to large momentum transfer, with fine energy resolution<sup>64</sup>. To facilitate the analysis of the INS data, the static structure factor  $S(Q)$  was measured separately using the NOMAD<sup>65</sup> diffractometer at the SNS. The results are similar for both alloys and will be illustrated mainly with the data

from  $Zr_{46}Cu_{46}Al_8$ . Meanwhile, MD simulations were performed for the  $Zr_{46}Cu_{46}Al_8$  MG with a realistic embedded atom method potential using the LAMMPS software package. The MD simulation results were benchmarked with the experimental  $S(Q)$ <sup>63</sup>. The vibration dynamics calculated by the MD simulations were analyzed in terms of the standard van Hove correlation function, which offered a direct comparison with INS measurements<sup>63</sup>. More details about the INS experiments and MD simulations can be found in Methods.

To investigate the momentum dependence of the BP, we first calculated the generalized  $\mathbf{Q}$ -dependent density of states (GDOS),  $G(\mathbf{Q}, E)$ , from the  $S(\mathbf{Q}, E)$  using the following equation<sup>59,63,66</sup>:

$$G(\mathbf{Q}, E) = e^{Q^2 u^2} \frac{E}{Q^2} \langle n \rangle S(\mathbf{Q}, E) \quad (1)$$

where  $\langle n \rangle = [1 - e^{-\frac{E}{k_B T}}]$  describes the Bose-Einstein statistics,  $u^2$  is the average vibrational mean-square displacement,  $e^{-Q^2 u^2}$  describes the Debye-Waller factor,  $k_B$  is the Boltzmann constant, and  $T$  the absolute temperature, respectively. In this paper, we defined a new quantity to further analyze the INS data. We divided  $G(\mathbf{Q}, E)$  by  $E^2$  to obtain  $B(\mathbf{Q}, E) = G(\mathbf{Q}, E)/E^2$ . Note that  $B(\mathbf{Q}, E)$  can be compared directly to  $g(E)/E^2$ , which is commonly used for the analysis of the BP<sup>17,18</sup>. In the Debye model<sup>20</sup>, the VDOS  $g(E) \propto E^2$  and thus  $g(E)/E^2$  becomes a constant at small  $E$  values. As shown in Fig. 1a, the spectra of  $B(\mathbf{Q}, E)$  from INS measurements exhibit a high concentration of INS intensities at  $E \sim 5.5$  meV around  $Q \sim 2.8 \text{ \AA}^{-1}$ . In MD simulations, Fig. 1b, the BP appears at  $E \sim 3.5$  meV, but the  $Q$ -dependence largely reproduces the experimental observations. Furthermore, in the vicinity of  $E \sim 5.5$  meV, the INS  $B(\mathbf{Q}, E)$  intensity exhibits a characteristic  $Q$ -dependence, which agrees well with the  $S(Q)$  measured separately with neutron diffraction, see Fig. 1c. This agreement is echoed by MD simulation results, Fig. 1d, which shows a nearly perfect correlation between  $B(\mathbf{Q}, E)$  and  $S(Q)$  at the BP energy.

Next, we demonstrate that the excitation around 5.5 meV corresponds to the energy of the BP. As shown in Fig. 2a, the INS measured total GDOS, obtained by integrating over a  $Q$  range of  $2.1\text{--}8.5 \text{ \AA}^{-1}$ , was normalized by  $E^2$ . An excess  $B(E)$  can be readily identified, centering around 5.5 meV for the  $Zr_{46}Cu_{46}Al_8$  MG under study. To solidify the evidence, two other experimental techniques were employed to confirm the BP energy in  $Zr_{46}Cu_{46}Al_8$  MG, i.e., Raman scattering and specific heat ( $C_p$ ) measurements. As shown in Fig. 2b, a clear BP around 6.0 meV in the reduced Raman spectra can be identified. This is consistent with the INS measured BP at  $\sim 5.5$  meV. Figure 2c plots the temperature dependence of  $C_p$ , in the form of  $(C_p - \gamma T)/T^3$  vs  $T$ , where  $\gamma$  is the Sommerfeld coefficient measuring the electronic contribution to  $C_p$ . As can be seen,  $(C_p - \gamma T)/T^3$  does not stay constant as predicted by the Debye model for crystalline materials<sup>67</sup>. However, adding an Einstein oscillator term (see Methods) leads to a good fit to the  $C_p$  data<sup>67</sup>. The fitted Einstein oscillator yields an average energy of  $\sim 6.2$  meV, which is also consistent with the BP energies obtained above. Note that the BPs in all three sets of data are broad, so there are uncertainties associated with fitting of the experimental data by each method, which is estimated to be 0.3–0.5 meV. Nonetheless, the largest discrepancy between the BP values determined by different methods is  $(6.2 \text{ meV} - 5.5 \text{ meV})/6.2 \text{ meV} \approx 11\%$ . With these three different measurements (i.e., INS, Raman scattering, and  $C_p$ ), we can thus confirm that the excitation at  $\sim 5.5$  meV in the INS spectra is indeed the BP.

Having established the BP, we performed a detailed analysis of the BP as a function of  $Q$ . For a given  $Q$  value between  $2.1$  and  $8.5 \text{ \AA}^{-1}$ , the constant  $Q$  cut plots of  $B(\mathbf{Q}, E)$  all show a BP anomaly (see Supplementary Fig. S1). Specifically, the BP peak position and peak height were extracted and examined to explore the momentum dependence of the energy and intensity of the BP, respectively. Interestingly, the BP energy for different  $Q$  values is quite similar, close to  $E \sim 5.5$  meV, which indicates that the BP is dispersionless, at least within the resolution of

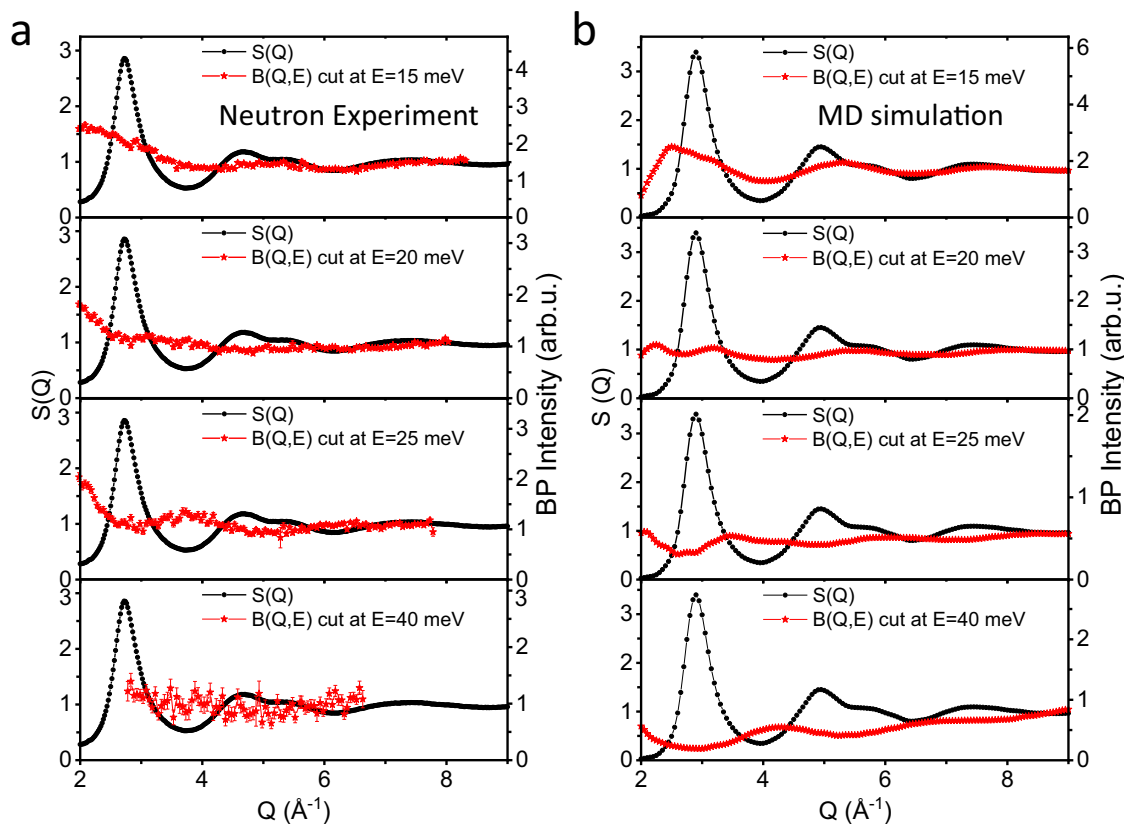


**Fig. 3 | Constant  $E$  cut plots of  $B(\mathbf{Q}, E)$  along with the static structure factor  $S(\mathbf{Q})$  in  $\text{Zr}_{46}\text{Cu}_{46}\text{Al}_8$  MG. **a** INS measurements. **b** MD simulations. Unlike at the BP excitation energy, the  $B(\mathbf{Q}, E)$  intensity at the indicated  $E$  values is not correlated**

with  $S(\mathbf{Q})$ . The error bars in (a) are estimated from the uncertainties of the measurement produced by the instrument software and propagated using the appropriate equation. Source data are provided in the Source Data file.

the ARCS instrument<sup>61</sup>. The lack of dispersion of the BP energy can also be seen in MD simulations at 3.5 meV, as shown in Fig. 1b. The BP energy of 3.5 meV in MD simulations is lower than the 5.5 meV determined by the INS experiment. We have conducted additional studies and confirmed that the lower BP energy value by MD simulations is not due to the simulation box size (see Supplementary Fig. S2). On the other hand, recent research by Su et al. has highlighted a significant increase in the BP energy with decreasing cooling rates<sup>68</sup>, indicating that the lower BP energy observed here could indeed be attributed to the high cooling rate employed in MD simulations. In spite of the difference in the BP energy values, the main features of the  $B(\mathbf{Q}, E)$  calculated by the MD simulations and INS experiment are largely the same, so a direct comparison can be made, and the results are discussed together.

Although the BP energy at different  $Q$  values is nearly constant at ~5.5 meV, the INS intensity at the BP energy varies strongly with  $Q$ . As shown in Fig. 1c, the momentum-dependent BP intensity shows a close one-to-one correspondence with  $S(\mathbf{Q})$ . This experimental observation was reproduced by MD simulations, as shown in Fig. 1d, demonstrating that the observed momentum dependence of the BP intensity is intrinsic. Apart from the results in Figs. 1c, d for  $\text{Zr}_{46}\text{Cu}_{46}\text{Al}_8$  MG, which is an excellent glass former, similar results were also obtained for  $\text{Zr}_{56}\text{Cu}_{36}\text{Al}_8$  MG with a marginal glass forming ability, in both INS measurements and MD simulations (see Supplementary Fig. S3). Taken together, the data from INS measurements and MD simulations for two different alloys of different glass-forming abilities would indicate that the BP excitation is closely connected with the underlying amorphous structures.

To further investigate the nature of the BP excitation, constant  $E$  cut plots of the BP spectra at selected  $E$  values were extracted and examined. Figure 3a shows the constant  $E$  cut plots of  $B(\mathbf{Q}, E)$  at  $E = 15, 20, 25,$  and  $40$  meV (over  $\Delta E = 0.5$  meV), respectively. The

corresponding MD simulation results are shown in Fig. 3b. No distinct correlations can be seen between  $S(\mathbf{Q})$  and constant  $E$  cut of  $B(\mathbf{Q}, E)$  at those energy values. For example, at  $E = 25$  meV, the maxima for the constant  $E$  cut of  $B(\mathbf{Q}, E)$  and  $S(\mathbf{Q})$  appear at different  $Q$  positions. The consistency between the INS experiments and MD simulations (Fig. 1) further confirms that the BP is a distinct excitation in the phonon spectra, different from phonons at other energies<sup>63</sup>. At the BP energy, the  $B(\mathbf{Q}, E)$  scales with the static structure factor,  $S(\mathbf{Q})$ .

A similar correlation of  $B(\mathbf{Q}, E)$  with  $S(\mathbf{Q})$  at the BP energy was also observed in MD simulation for a 3-dimensional Lennard-Jones (3DLJ) and a 3-dimensional power law (3DPL) binary glasses. The simulation results are shown in Supplementary Fig. S4, which confirms two main features of the BP: (1) the BP energy is largely dispersionless, and (2) the  $B(\mathbf{Q}, E)$  intensity scales with  $S(\mathbf{Q})$ . These findings, based on the simulation with a generic 3DLJ potential and 3DPL potential, suggest that the BP features reported here are not limited to specific cases but might represent a universal feature in glasses.

Based on INS and MD simulation results, an analytical form for the BP in amorphous materials can be formulated:

$$B_{BP}(\mathbf{Q}, E) = A * f(E - E_{BP}) S(\mathbf{Q}) \quad (2)$$

where  $A$  is a scaling factor, and the function  $f(E - E_{BP})$  is momentum-independent which has a peak at  $E = E_{BP}$  that describes the dispersionless feature of the BP energy. It follows that the corresponding dynamic structure factor of the BP can be written as:

$$S_{BP}(\mathbf{Q}, E) = A * EQ^2 e^{-Q^2 u^2} \langle n \rangle^{-1} f(E - E_{BP}) S(\mathbf{Q}) \quad (3)$$

A step-by-step derivation can be found in Supplementary Materials.

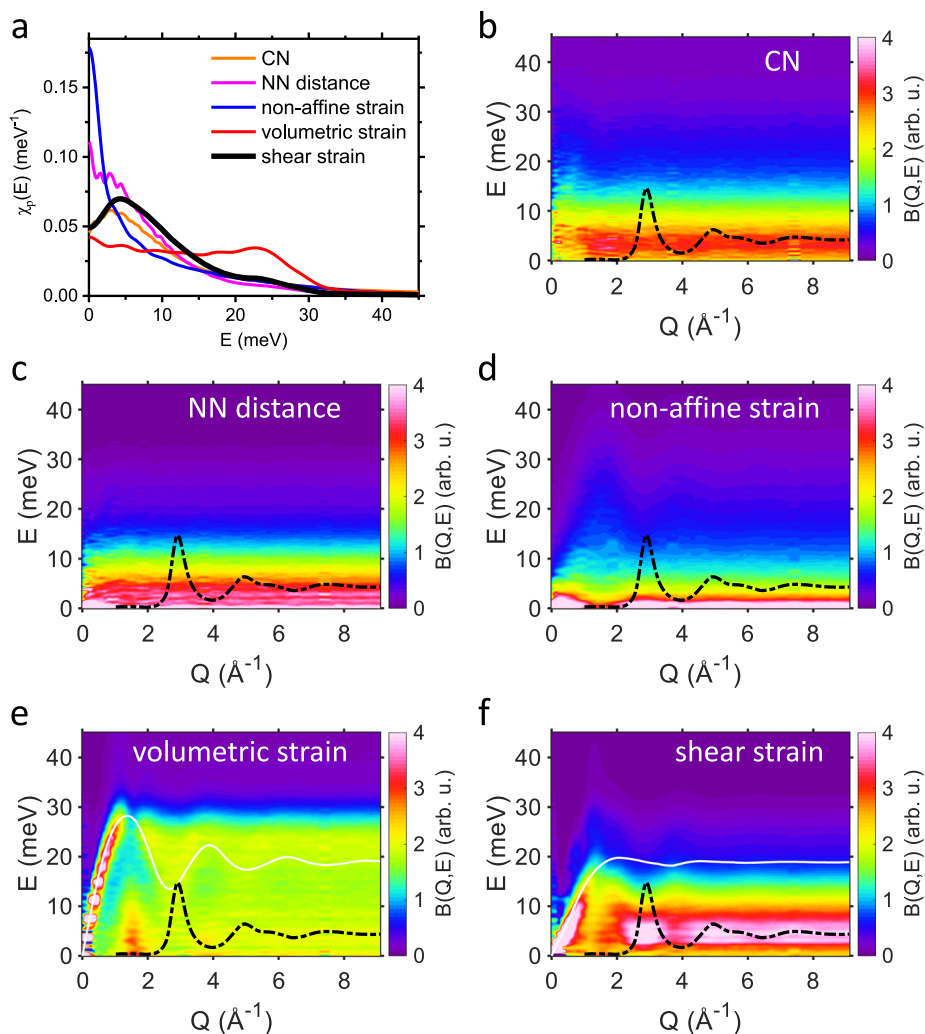


**Fig. 4 | The  $Q$ -dependent frequency spectrum resulting from various structure fluctuations in  $Zr_{46}Cu_{46}Al_8$  MG. **a** The  $Q$ -integrated frequency spectrum, which reflects the density of states. **b** The local coordination number (CN) fluctuation model, which shows a dispersionless BP but not  $S(Q)$ -like BP intensity. **c** The nearest-neighbor (NN) distance fluctuation model, which shows neither a dispersionless BP nor  $S(Q)$ -like BP intensity. **d** The non-affine strain model, which shows  $S(Q)$ -like BP intensity but not the gapped dispersionless BP energy. **e** The**

volumetric strain model, which shows none of the observed BP features. **f** The shear strain model, which shows a dispersionless BP and  $S(Q)$ -like BP intensity at  $E \sim 4.3$  meV, capturing the main features observed in the INS experiment and MD simulations as shown in Fig. 1. Note that the volumetric strain and shear strain model respectively produced the longitudinal and transverse phonon dispersions (white curves in (e) and (f)) which we reported in ref. 63. The  $S(Q)$  was superimposed as black dashed lines. Source data are provided in the Source Data file.

Previous studies of the BP have primarily focused on the energy-dependent DOS, which is the Fourier transform of the time-dependent velocity autocorrelation function, e.g.,  $g(\omega) = \frac{1}{2\pi} \int \frac{\psi_v(t)}{\psi_v(0)} \exp(-i\omega t) dt$ , where  $\psi_v(t) = N^{-1} \sum_j \langle \mathbf{v}_{j,t} \cdot \mathbf{v}_{j,0} \rangle$ . Guerdane and Teichler generalized the definition of the autocorrelation function by replacing the atomic velocity with fluctuations of atomic coordination number (CN), i.e.,  $\psi_{CN}(t) = N^{-1} \sum_j \langle (Z_{j,t} - \bar{Z}_j)(Z_{j,0} - \bar{Z}_j) \rangle$ <sup>54</sup>. The Fourier transform  $\chi_{CN}(\omega) = \frac{1}{2\pi} \int \frac{\psi_{CN}(t)}{\psi_{CN}(0)} \exp(-i\omega t) dt$  can be treated as a DOS, describing the oscillation frequency of atomic CN. They found that  $\chi_{CN}(E)$ , where  $E = \hbar\omega$  with  $\hbar$  being the reduced Planck constant, shows a clear peak at  $E$  around  $E_{BP}$ , and thus concluded that the BP is related to time-dependent fluctuations of local environments of atoms.

To describe the  $Q$ -dependence, we consider the double Fourier transform of the spatial correlation of CN fluctuations between different atoms. The correlation function can be extended as:

$$\varphi_{CN}(\mathbf{Q}, t) = N^{-1} \sum_j \sum_k \langle (Z_{j,t} - \bar{Z}_j)(Z_{k,0} - \bar{Z}_k) e^{i\mathbf{Q} \cdot (\mathbf{r}_{j,t} - \mathbf{r}_{k,0})} \rangle \quad (4)$$

Then, the generalized  $Q$ -dependent DOS for CN fluctuation follows:

$$\Omega_{CN}(\mathbf{Q}, \omega) = \frac{1}{2\pi} \int \frac{\varphi_{CN}(\mathbf{Q}, t)}{\varphi_{CN}(\mathbf{Q}, 0)} e^{-i\omega t} dt \quad (5)$$

As shown in Fig. 4a,  $\chi_{CN}(E)$  exhibits a clear peak around the BP energy in  $Zr_{46}Cu_{46}Al_8$  MG, which is consistent with a previous study<sup>54</sup>. However, as Fig. 4b shows, the  $Q$ -dependent  $\Omega_{CN}(\mathbf{Q}, E)$  did not produce the  $S(Q)$ -like feature observed in the INS experiment and MD simulations (Fig. 1).

To further explore the underlying physics of the BP, we went on to study the spatial and temporal fluctuations of several other parameters, such as the nearest-neighbor (NN) distance and local atomic strain, by using Eq. (4, 5) (see “Methods”). Previous studies have shown that the fluctuation of the NN distance is closely linked to the variation of force constants, which has been assumed to be the origin of BP<sup>22</sup>. However, as Fig. 4c, a demonstrate, it captures neither the BP energy nor the  $S(Q)$ -like feature of BP intensity. The local atomic strain can be

decomposed into three terms: the non-affine strain, the volumetric strain, and the shear strain<sup>69</sup>. Their double Fourier transforms are shown in Fig. 4(d–f). Interestingly, only the shear strain fluctuation produces both the  $E$  and  $Q$  dependence of the BP as observed by our INS experiment and MD simulations (Fig. 1). Fluctuations of the non-affine strain and volumetric strain did not show such correlations. These simulation results strongly suggest that BP is intimately associated with the fluctuation of the local shear strain around each atom due to topological disorder. In the future, fluctuations of other order parameters could also be checked in a similar way. The above analysis also serves as a reminder that an apparent peak in the energy-dependent DOS does not necessarily correspond to the BP.

## Discussion

In a previous MD simulation study<sup>42</sup>, Shintani and Tanaka posit that the BP is related to the Ioffe-Regel limit of transverse phonons and is solely characterized by an energy scale, unrelated to any real-space length scale. Hu and Tanaka<sup>13</sup> recently further explored this idea with MD simulations of a 2D model glass by demonstrating the dispersionless feature of the BP, emphasizing its localized nature (no characteristic  $Q$  or length scale). On the other hand, Lerner et al. studied the same 2D glass system but suggested that the BP is a hybridized mode of phononic and four-leaf quasilocated excitations<sup>70</sup>. Our study, which is based on INS experimental observation and accompanying MD simulations, suggests that the BP in MG is due to the fluctuation of the local shear deformation. The one-to-one correspondence between  $B(\mathbf{Q}, E)$  and  $S(Q)$  indicates that the BP is intimately related to the underlying amorphous structure of the material. Our study also demonstrates that the momentum dependence of the BP intensity is essential to establishing the nature of the BP, and needs to be systematically characterized in future studies.

There has been a long debate as to whether the BP in amorphous materials is related to the van Hove singularity in its crystalline counterpart<sup>36,71</sup>. Chumakov et al. reported that as the applied pressure increases, the BP energy spectrum tends to approach the van Hove singularity of the transverse acoustic phonon of the crystalline counterpart, leading to the conclusion of their equivalence<sup>36</sup>. On the other hand, a recent light experiment and a comprehensive MD simulation study of a real 2D model glass by Wang et al. suggests that the BP and van Hove singularity are two separate physical phenomena<sup>71</sup>. Therefore, whether and how the BP is related to van Hove singularity remains an open question<sup>18</sup> and a fertile ground of future research.

We noticed that earlier published works adopted different expressions of  $S(\mathbf{Q}, E)$ , namely  $S(\mathbf{Q}, E)^*E/Q$ , or  $S(\mathbf{Q}, E)^*n > / (E^*Q)$  for BP<sup>17,39,59</sup>, to examine the  $Q$ -dependence of the INS data. We also calculated these quantities and compared the results with  $B(\mathbf{Q}, E)$ , as shown in Supplementary Fig. S5. While the explicit values differ, a  $Q$ -dependent feature can be seen for  $S(\mathbf{Q}, E)$  and  $S(\mathbf{Q}, E)^*n > / (E^*Q)$  around the BP energy.

In summary, by interrogating the momentum dependence of INS and MD simulation results, we have established important characteristics of the BP in amorphous alloys. We found that the BP excitation is essentially dispersionless, i.e., with a fixed energy. In addition, a one-to-one correspondence was found between the INS intensity (represented in the form of  $B(\mathbf{Q}, E)$ ) at the BP excitation energy and the static structure factor  $S(Q)$ , and this was reproduced by MD simulations with calibrated empirical potentials. These features could be fingerprints to distinguish the origin of the BP in amorphous materials from those observed in other systems. A simple analytical expression describing the dynamic structure factor of the BP excitation has been formulated for the MG under study. Inspired by the experimental observations, we found, through MD simulations, that fluctuations of the local atomic shear strain reproduce both the dispersionless feature of the BP energy and the momentum-dependent BP intensity. We also ruled out four other models involving fluctuations by the local CN, the NN distance,

the non-affine strain, and the volumetric strain. Although the present study was demonstrated for MGs, the same methodology could be applied to other types of glasses. The powerful combination of INS and MD not only shed light on the nature of the BP but also pointed out the importance of considering shear strain fluctuations for understanding the dynamic properties of amorphous materials.

## Methods

### Sample synthesis

Amorphous alloy ingots with compositions of  $Zr_{46}Cu_{46}Al_8$  and  $Zr_{56}Cu_{36}Al_8$  MGs were prepared by arc melting a mixture of Zr (99.99%), Cu (99.99%), and Al (99.99%) in appropriate amounts under a Ti-gettered Ar atmosphere. Each ingot was re-melted six times to ensure compositional homogeneity and quenched into copper-mold by suction casting under a high-purity Ar atmosphere. The cooling rate was estimated to be ~ 20 K/min.

### Neutron Total Scattering Measurements

Neutron total scattering measurements were carried out to determine the static structure factor,  $S(Q)$ , in  $Zr_{46}Cu_{46}Al_8$  and  $Zr_{56}Cu_{36}Al_8$  MGs at room temperature (RT) using the Nanoscale-Ordered Materials Diffractometer (NOMAD<sup>65</sup>) at the Spallation Neutron Source (SNS), Oak Ridge National Laboratory (ORNL), USA.

### Inelastic neutron scattering

The INS experiment was carried out to measure the atomic dynamics in  $Zr_{46}Cu_{46}Al_8$  and  $Zr_{56}Cu_{36}Al_8$  MGs, using the time-of-flight wide Angular-Range Chopper Spectrometer (ARCS<sup>61</sup>) at the SNS, ORNL, USA. The measurements were performed with an incident neutron energy of  $E_i = 50$  meV at RT. The dynamic structure factor,  $S(\mathbf{Q}, E)$ , where  $\mathbf{Q}$  and  $E$  are the neutron momentum and energy transfer, respectively, was generated using the standard software MantidPlot<sup>72</sup>.

### Raman scattering

Raman spectra were measured at RT with a Horiba micro Raman system in  $Zr_{46}Cu_{46}Al_8$  MG. A 532 nm laser was used for excitation with a power of 1 mW to avoid sample damage. An 1800 lines/mm grating was used in the Raman measurements, which enables each CCD pixel to cover  $0.52 \text{ cm}^{-1}$  at 2.33 eV. The laser line was removed by using three BraggGrate notch filters with a spectral bandwidth of 5–10  $\text{cm}^{-1}$ . From the Raman scattering intensity  $I(E)$ , the DOS was reduced following  $I(E)/E/[n(E)+1] = C(E)*g(E)/E^2$ , where  $C(E)$  is the coupling coefficient of the vibrational mode to the light, and  $n(E) = 1/[e^{E/k_B T} - 1]$  is the Bosons occupation number<sup>25</sup>. In this study,  $C(E) = \text{constant}$  was used for the following reason. Shuker and Gammon<sup>73</sup> predicted  $C(E) = \text{constant}$  by assuming that vibrations are localized on a distance much shorter than the light wavelength in amorphous materials. The results shown in Fig. 4 suggest that the local shear strain fluctuations are in the 0.1–1 nm scale. The Raman scattering experiment used 532 nm laser which is much longer than the length scale of local shear strain fluctuations. Thus, a constant coupling factor was deemed appropriate for the Raman scattering data analysis. The Raman scattering measured BP is ~ 6 meV (Fig. 2b), slightly higher than that determined by the INS (Fig. 2a). It is noted that the Raman BP energy will shift to a lower value if a linear relationship is assumed between  $C(E)$  and  $E$ <sup>18,74,75</sup>.

### Specific heat

Specific heat  $C_p$  measurements were performed on  $Zr_{46}Cu_{46}Al_8$  MG with a sample mass of 3.6 mg using a Quantum Design Physical Property Measurement System (PPMS) for temperatures ranging from 5 to 100 K.  $C_p$  was fitted as  $C_p = \gamma T + n_D C_D + \int_0^\infty n_E C_E \cdot \chi_E(\theta_E, \bar{\theta}_E, \sigma_E) d\theta_E$ , where  $\gamma T$  is mainly contributed by free electrons,  $n_D$  and  $n_E$  represent the fractions of the conventional phonon mode (Debye mode) and

Einstein mode, respectively,  $C_D = 9R(T/\theta_D)^3 \int_0^{\theta_D/T} \frac{\zeta^4 e^\zeta}{(e^\zeta - 1)^2} d\zeta$  and  $C_E = 3R(\theta_E/T)^2 \frac{e^{\theta_E/T}}{(e^{\theta_E/T} - 1)^2}$  are their heat capacities of the phonon and Einstein modes, respectively, where  $\theta_D$  is Debye temperature.  $\chi_E(\theta_E, \bar{\theta}_E, \sigma_E) = \frac{1}{\sqrt{2\pi}\sigma_E} \exp[-\frac{(\theta_E - \bar{\theta}_E)^2}{2\sigma_E^2}]$  is energy distribution of the Einstein oscillator, where  $\bar{\theta}_E$  and  $\sigma_E$  are the mean and standard deviation of the distribution, respectively<sup>67</sup>. The total VDOS for the phonon and Einstein modes can be expressed as  $g(E) = 3N(n_D \cdot \frac{3E^2}{(k_B\theta_D)^3} + n_E \cdot \chi_E(\theta_E, \bar{\theta}_E, \sigma_E)/k_B)$ , where  $N$  is Avogadro's number<sup>76</sup>. The BP can be extracted from the  $g(E)/E^2$  data, which gives the BP energy from  $C_p$ . The fact that Einstein mode is needed to model the specific heat data is suggestive of a localized harmonic vibration mode. The Gaussian distribution of Einstein mode suggests the topologically diverse form of vibration modes, which randomly occur without interactions<sup>67,76</sup>. The Debye level of the Debye mode contribution is also plotted in Fig. 2c.

### Molecular dynamics (MD) simulations

In this work, classical MD simulations were performed to investigate the atomic structures and vibrational dynamics of ternary  $Zr_{46}Cu_{46}Al_8$  and  $Zr_{56}Cu_{36}Al_8$  MGs within the LAMMPS package (lammmps-3Mar2020). The interatomic interactions were described by a realistic embedded-atom method (EAM) potential developed by Sheng et al.<sup>77</sup>. In brief, the potential energy of atom  $i$  is divided into two contributions: a pairwise part and a local density part:

$$E_i = F_\alpha \left( \sum_{j \neq i} \rho_\beta(r_{ij}) \right) + \frac{1}{2} \sum_{j \neq i} \phi_{\alpha\beta}(r_{ij})$$

where  $\alpha$  and  $\beta$  are the element types of the center (embedded) atom  $i$  and the neighboring atom  $j$ .  $\rho_\beta$  is the charge density function of  $\beta$ ,  $F_\alpha$  is the embedding function of  $\alpha$ ,  $\phi_{\alpha\beta}$  is the pair potential function between  $\alpha$  and  $\beta$ . The total potential energy of the system is the summation of the potential energy of each atom. We simulated the system containing 10000 atoms in a cubic box with periodic boundary conditions applied in three directions. In the process of sample preparation, the sample was first melted and equilibrated at 2000 K for 2.0 ns (MD time step is 2.0 fs), followed by hyper-quenching to 300 K with a cooling rate of  $10^{12}$  K/s, then relaxed for 2.0 ns at 300 K. In this process, the isobaric and isothermal (NPT) ensemble was used with the sample size being adjusted to give zero pressure. After that, the canonical (NVT) ensemble MD was conducted at 300 K for data collection and analysis (Supplementary Data 1). The simulated static structure factor of  $Zr_{46}Cu_{46}Al_8$  MG was benchmarked with experimental measurements<sup>63</sup>. A good agreement is demonstrated.

### Data availability

All data needed to evaluate the conclusions in the paper are available in the article or the Supplementary Information. Raw neutron scattering data acquired in this study are preserved indefinitely at SNS, ORNL, USA. The experimental and simulation data generated in this study are provided in the Source Data file. All the raw data relevant to the study are available from the corresponding author upon request. Source data are provided in this paper.

### References

- Zhong, L., Wang, J., Sheng, H., Zhang, Z. & Mao, S. X. Formation of monatomic metallic glasses through ultrafast liquid quenching. *Nature* **512**, 177–180 (2014).
- Debenedetti, P. G. & Stillinger, F. H. Supercooled liquids and the glass transition. *Nature* **410**, 259–267 (2001).
- Angell, C. A. Formation of Glasses from Liquids and Biopolymers. *Science* **267**, 1924–1935 (1995).
- Wang, W. H. Dynamic relaxations and relaxation-property relationships in metallic glasses. *Prog. Mater. Sci.* **106**, 100561 (2019).
- Angell, C. A., Ngai, K. L., McKenna, G. B., McMillan, P. F. & Martin, S. W. Relaxation in glassforming liquids and amorphous solids. *J. Appl. Phys.* **88**, 3113–3157 (2000).
- Chen, Y. et al. Visualizing slow internal relaxations in a two-dimensional glassy system. *Nat. Phys.* **19**, 969–977 (2023).
- Ruiz-Ruiz, M. et al. Real-time microscopy of the relaxation of a glass. *Nat. Phys.* **19**, 1509–1515 (2023).
- Ghanekarade, A., Phan, A. D., Schweizer, K. S. & Simmons, D. S. Signature of collective elastic glass physics in surface-induced long-range tails in dynamical gradients. *Nat. Phys.* **19**, 800–806 (2023).
- Guiselin, B., Scalliet, C. & Berthier, L. Microscopic origin of excess wings in relaxation spectra of supercooled liquids. *Nat. Phys.* **18**, 468–472 (2022).
- Chang, C. et al. Liquid-like atoms in dense-packed solid glasses. *Nat. Mater.* **21**, 1240–1245 (2022).
- Song, S., Zhu, F. & Chen, M. Universal scaling law of glass rheology. *Nat. Mater.* **21**, 404–409 (2022).
- Li, B., Lou, K., Kob, W. & Granick, S. Anatomy of cage formation in a two-dimensional glass-forming liquid. *Nature* **587**, 225–229 (2020).
- Hu, Y.-C. & Tanaka, H. Origin of the boson peak in amorphous solids. *Nat. Phys.* **18**, 669–677 (2022).
- Wang, W. H., Yang, Y., Nieh, T. G. & Liu, C. T. On the source of plastic flow in metallic glasses: Concepts and models. *Intermetallics* **67**, 81–86 (2015).
- Takabatake, T., Suekuni, K., Nakayama, T. & Kaneshita, E. Phonon-glass electron-crystal thermoelectric clathrates: Experiments and theory. *Rev. Mod. Phys.* **86**, 669–716 (2014).
- Schwabl, F. *Advanced Quantum Mechanics*. (Springer Berlin Heidelberg, 2008).
- Nakayama, T. Boson peak and terahertz frequency dynamics of vitreous silica. *Reports Prog. Phys.* **65**, 1195–1242 (2002).
- Ramos, M. A. *Low-Temperature Thermal and Vibrational Properties of Disordered Solids*. (WORLD SCIENTIFIC (EUROPE), 2022).
- Frick, B. & Richter, D. The microscopic basis of the glass transition in polymers from neutron scattering studies. *Science* **267**, 1939–1945 (1995).
- Grigera, T. S., Martin-Mayor, V., Parisi, G. & Verrocchio, P. Phonon interpretation of the ‘boson peak’ in supercooled liquids. *Nature* **422**, 289–292 (2003).
- Greaves, G. N., Meneau, F., Majérus, O., Jones, D. G. & Taylor, J. Identifying vibrations that destabilize crystals and characterize the glassy state. *Science* **308**, 1299–1302 (2005).
- Kaya, D., Green, N. L., Maloney, C. E. & Islam, M. F. Normal modes and density of states of disordered colloidal solids. *Science* **329**, 656–658 (2010).
- Phillips, W. A. *Amorphous Solids Low Temperature Properties*. (Springer Berlin Heidelberg, 1981).
- Uchino, T. & Yoko, T. Low-frequency raman scattering and the fast relaxation process in glycerol. *Science* **273**, 480–483 (1996).
- Malinovsky, V. K. & Sokolov, A. P. The nature of boson peak in Raman scattering in glasses. *Solid State Commun.* **57**, 757–761 (1986).
- Tong, P. et al. Structural irreversibility and enhanced brittleness under fatigue in Zr-based amorphous solids. *Metals (Basel)* **2**, 529–539 (2012).
- Sette, F., Krisch, M. H., Masciovecchio, C., Ruocco, G. & Monaco, G. Dynamics of glasses and glass-forming liquids studied by inelastic X-ray scattering. *Science* **280**, 1550–1555 (1998).
- Baldi, G., Giordano, V. M., Monaco, G. & Ruta, B. Sound attenuation at terahertz frequencies and the boson peak of vitreous silica. *Phys. Rev. Lett.* **104**, 195501 (2010).

29. Krishnan, R. S. The scattering of light in fused quartz and its Raman spectrum. *Proc. Indian Acad. Sci. Sect. A* **37**, 377–384 (1953).
30. Zeller, R. C. & Pohl, R. O. Thermal conductivity and specific heat of noncrystalline solids. *Phys. Rev. B* **4**, 2029–2041 (1971).
31. Zhang, H. P., Fan, B. B., Wu, J. Q., Wang, W. H. & Li, M. Z. Universal relationship of boson peak with Debye level and Debye-Waller factor in disordered materials. *Phys. Rev. Mater.* **4**, 095603 (2020).
32. Yang, J. et al. Structural parameter of orientational order to predict the boson vibrational anomaly in glasses. *Phys. Rev. Lett.* **122**, 015501 (2019).
33. Inoue, K. et al. Low-energy excitations in amorphous polymers. *J. Chem. Phys.* **95**, 5332–5340 (1991).
34. González-Jiménez, M. et al. Understanding the emergence of the boson peak in molecular glasses. *Nat. Commun.* **14**, 215 (2023).
35. Nemanich, R. J. Low-frequency inelastic light scattering from chalcogenide glasses and alloys. *Phys. Rev. B* **16**, 1655–1674 (1977).
36. Chumakov, A. I. et al. Equivalence of the boson peak in glasses to the transverse acoustic van hove singularity in crystals. *Phys. Rev. Lett.* **106**, 225501 (2011).
37. Ando, M. F. et al. Boson peak, heterogeneity and intermediate-range order in binary SiO<sub>2</sub>-Al<sub>2</sub>O<sub>3</sub> glasses. *Sci. Rep.* **8**, 5394 (2018).
38. Baldi, G. et al. Thermal conductivity and terahertz vibrational dynamics of vitreous silica. *Phys. Rev. B* **77**, 214309 (2008).
39. Kofu, M. et al. Inelastic neutron scattering study on boson peaks of imidazolium-based ionic liquids. *J. Mol. Liq.* **210**, 164–168 (2015).
40. Kabeya, M. et al. Boson peak dynamics of glassy glucose studied by integrated terahertz-band spectroscopy. *Phys. Rev. B* **94**, 224204 (2016).
41. Zhang, L. et al. Experimental studies of vibrational modes in a two-dimensional amorphous solid. *Nat. Commun.* **8**, 67 (2017).
42. Shintani, H. & Tanaka, H. Universal link between the boson peak and transverse phonons in glass. *Nat. Mater.* **7**, 870–877 (2008).
43. Taraskin, S. N., Loh, Y. L., Natarajan, G. & Elliott, S. R. Origin of the boson peak in systems with lattice disorder. *Phys. Rev. Lett.* **86**, 1255–1258 (2001).
44. Wang, L. et al. Low-frequency vibrational modes of stable glasses. *Nat. Commun.* **10**, 26 (2019).
45. Mallamace, F. et al. The Boson peak interpretation and evolution in confined amorphous water. *Sci. China Phys. Mech. Astron.* **62**, 107004 (2019).
46. Wang, Z. et al. Boson peak in deeply cooled confined water: a possible way to explore the existence of the liquid-to-liquid transition in water. *Phys. Rev. Lett.* **112**, 237802 (2014).
47. Ren, S. et al. Boson-peak-like anomaly caused by transverse phonon softening in strain glass. *Nat. Commun.* **12**, 5755 (2021).
48. Szewczyk, D. et al. Heat capacity anomalies of the molecular crystal 1-fluoro-adamantane at low temperatures. *Sci. Rep.* **11**, 18640 (2021).
49. Hansen, H. W., Sanz, A., Adrjanowicz, K., Frick, B. & Niss, K. Evidence of a one-dimensional thermodynamic phase diagram for simple glass-formers. *Nat. Commun.* **9**, 518 (2018).
50. Kofu, M. et al. Spin glass behavior and magnetic boson peak in a structural glass of a magnetic ionic liquid. *Sci. Rep.* **11**, 12098 (2021).
51. Lubchenko, V. & Wolynes, P. G. The origin of the boson peak and thermal conductivity plateau in low-temperature glasses. *Proc. Natl. Acad. Sci. USA* **100**, 1515–1518 (2003).
52. Scopigno, T., Suck, J.-B. B., Angelini, R., Albergamo, F. & Ruocco, G. High-frequency dynamics in metallic glasses. *Phys. Rev. Lett.* **96**, 135501 (2006).
53. Schirmacher, W., Diezemann, G. & Ganter, C. Harmonic vibrational excitations in disordered solids and the “boson peak”. *Phys. Rev. Lett.* **81**, 136–139 (1998).
54. Guerdane, M. & Teichler, H. Short-range-order lifetime and the “boson peak” in a metallic glass model. *Phys. Rev. Lett.* **101**, 065506 (2008).
55. Buchenau, U., Nücker, N. & Dianoux, A. J. Neutron scattering study of the low-frequency vibrations in vitreous silica. *Phys. Rev. Lett.* **53**, 2316–2319 (1984).
56. Buchenau, U. et al. Low-frequency modes in vitreous silica. *Phys. Rev. B* **34**, 5665–5673 (1986).
57. Buchenau, U., Zhou, H. M., Nücker, N., Gilroy, K. S. & Phillips, W. A. Structural relaxation in vitreous silica. *Phys. Rev. Lett.* **60**, 1318–1321 (1988).
58. Nakamura, M., Arai, M., Otomo, T., Inamura, Y. & Bennington, S. M. Dispersive excitation in different forms of SiO<sub>2</sub>. *J. Non. Cryst. Solids* **293–295**, 377–382 (2001).
59. Arai, M., Inamura, Y. & Otomo, T. Novel dynamics of vitreous silica and metallic glass. *Philos. Mag. B* **79**, 1733–1739 (1999).
60. Ruocco, G. & Sette, F. High-frequency vibrational dynamics in glasses. *J. Phys. Condens. Matter* **13**, 9141–9164 (2001).
61. Abernathy, D. L. et al. Design and operation of the wide angular-range chopper spectrometer ARCS at the Spallation Neutron Source. *Rev. Sci. Instrum.* **83**, 015114 (2012).
62. Scopigno, T., Ruocco, G. & Sette, F. Microscopic dynamics in liquid metals: The experimental point of view. *Rev. Mod. Phys.* **77**, 881–933 (2005).
63. Li, X. Y. et al. Observation of high-frequency transverse phonons in metallic glasses. *Phys. Rev. Lett.* **124**, 225902 (2020).
64. Stone, M. B. et al. A comparison of four direct geometry time-of-flight spectrometers at the Spallation Neutron Source. *Rev. Sci. Instrum.* **85**, 045113 (2014).
65. Neuefeind, J., Feygenson, M., Carruth, J., Hoffmann, R. & Chipley, K. K. The nanoscale ordered MAterials diffractometer NOMAD at the spallation neutron source SNS. *Nucl. Instruments Methods Phys. Res. Sect. B Beam Interact. with Mater. Atoms* **287**, 68–75 (2012).
66. Carpenter, J. M. & Price, D. L. Correlated motions in glasses studied by coherent inelastic neutron scattering. *Phys. Rev. Lett.* **54**, 441–443 (1985).
67. Huang, B. et al. Hand in hand evolution of boson heat capacity anomaly and slow  $\beta$ -relaxation in La-based metallic glasses. *Acta Mater* **110**, 73–83 (2016).
68. Su, R. et al. Atomic origin of annealing embrittlement in metallic glasses. Preprint at <https://doi.org/10.48550/arXiv.2208.13747> (2022).
69. Falk, M. L. & Langer, J. S. Dynamics of viscoplastic deformation in amorphous solids. *Phys. Rev. E* **57**, 7192–7205 (1998).
70. Lerner, E. & Bouchbinder, E. Boson-peak vibrational modes in glasses feature hybridized phononic and quasilocated excitations. *J. Chem. Phys.* **158**, 194503 (2023).
71. Wang, Y., Hong, L., Wang, Y., Schirmacher, W. & Zhang, J. Disentangling boson peaks and Van Hove singularities in a model glass. *Phys. Rev. B* **98**, 174207 (2018).
72. Arnold, O. et al. Mantid—Data analysis and visualization package for neutron scattering and  $\mu$ SR experiments. *Nucl. Instruments Methods Phys. Res. Sect. A Accel. Spectrometers, Detect. Assoc. Equip.* **764**, 156–166 (2014).
73. Shuker, R. & Gammon, R. W. Raman-scattering selection-rule breaking and the density of states in amorphous materials. *Phys. Rev. Lett.* **25**, 222–225 (1970).
74. Surovtsev, N. V. & Sokolov, A. P. Frequency behavior of raman coupling coefficient in glasses. *Phys. Rev. B* **66**, 054205 (2002).
75. Surovtsev, N. V., Shebanin, A. P. & Ramos, M. A. Density of states and light-vibration coupling coefficient in B<sub>2</sub>O<sub>3</sub> glasses with different thermal history. *Phys. Rev. B* **67**, 024203 (2003).
76. Huang, B., Bai, H. Y. & Wang, W. H. Relationship between boson heat capacity peaks and evolution of heterogeneous structure in metallic glasses. *J. Appl. Phys.* **115**, 153505 (2014).
77. Cheng, Y. Q., Ma, E. & Sheng, H. W. Atomic level structure in multicomponent bulk metallic glass. *Phys. Rev. Lett.* **102**, 245501 (2009).

## Acknowledgements

X.L.W., X.Y.L., C.H.H., and L.R.F. thank the support by the Research Grants Council of the Hong Kong Special Administrative Region, China (Project No. JLF5/P-101/24), a grant at City University of Hong Kong (Project No. 9229019), and Croucher Senior Research Fellowship (CityU Project No. 9500008). X.L.W. and S.L. acknowledge support by the NSFC/RGC Joint Research Scheme (No. N\_CityU173/22) and Guangdong-Hong Kong-Macao Joint Laboratory for Neutron Scattering Science and Technology (grant no. 2019B121205003). S.L. acknowledges support by the National Natural Science Foundation of China (No. 12261160364, 52222104). M.Z.L. acknowledges support by the National NSFC (Nos. 52031016, 12574220, and 51631003). H.P.Z. acknowledges support by the National NSFC (Nos. 52301214 and 52192601). The neutron scattering experiments were carried out at the Spallation Neutron Source, which is sponsored by the Scientific User Facilities Division, Office of Basic Energy Sciences, US Department of Energy, under contract No. DE-AC05-00OR22725 with Oak Ridge National Laboratory.

## Author contributions

X.L.W., X.Y.L., S.L. and D.L.A. designed and performed the inelastic neutron scattering experiment using ARCS at the SNS, with samples prepared by S.L. X.Y.L. analyzed the ARCS data, along with H.P.Z., S.L., D.L.A., M.Z.L., and X.L.W. H.P.Z. and M.Z.L. performed the MD simulations. S.L. performed the neutron total scattering experiment using NOMAD at the SNS. X.Y.L., H.P.Z., M.Z.L., and X.L.W. drafted the manuscript. X.Y.L., H.P.Z., S.L., D.L.A., C.H.H., L.R.F., M.Z.L., and X.L.W. analyzed and reviewed the results and provided input to this paper. X.L.W. conceived and supervised the project.

## Competing interests

The authors declare no competing interests.

## Additional information

**Supplementary information** The online version contains supplementary material available at <https://doi.org/10.1038/s41467-025-67574-y>.

**Correspondence** and requests for materials should be addressed to M. Z. Li or X.-L. Wang.

**Peer review information** *Nature Communications* thanks the anonymous reviewer(s) for their contribution to the peer review of this work. A peer review file is available.

**Reprints and permissions information** is available at <http://www.nature.com/reprints>

**Publisher's note** Springer Nature remains neutral with regard to jurisdictional claims in published maps and institutional affiliations.

**Open Access** This article is licensed under a Creative Commons Attribution-NonCommercial-NoDerivatives 4.0 International License, which permits any non-commercial use, sharing, distribution and reproduction in any medium or format, as long as you give appropriate credit to the original author(s) and the source, provide a link to the Creative Commons licence, and indicate if you modified the licensed material. You do not have permission under this licence to share adapted material derived from this article or parts of it. The images or other third party material in this article are included in the article's Creative Commons licence, unless indicated otherwise in a credit line to the material. If material is not included in the article's Creative Commons licence and your intended use is not permitted by statutory regulation or exceeds the permitted use, you will need to obtain permission directly from the copyright holder. To view a copy of this licence, visit <http://creativecommons.org/licenses/by-nc-nd/4.0/>.

© The Author(s) 2025